Properties of multiferroic $BiFeO_3$ under high magnetic fields from first principles

S. Lisenkov,[1] Igor A. Kornev,[1,2] and L. Bellaiche[1]
[1]*Department of Physics, University of Arkansas, Fayetteville, Arkansas 72701, USA*
[2]*Mads Clausen Institute for Product Innovation, University of Southern Denmark, Alsion 2, DK-6400 Sonderborg, Denmark*
(Received 28 November 2008; published 8 January 2009)

Properties of $BiFeO_3$ under high magnetic fields applied in the plane perpendicular to the polarization are investigated via an original first-principles-based effective Hamiltonian. Different phenomena are found, depending if the magnetic fields lie (a) along the initial direction of the antiferromagnetic vector, (b) perpendicular to it, or (c) in between these two latter directions. For instance, a spin-flop transition occurs for case (a), while a continuous transition occurs, for which both the antiferromagnetic vector and the field-induced magnetization rotate, for case (c). Such latter rotation leads to a controllable large enhancement of the magnetoelectric coefficient.

DOI: 10.1103/PhysRevB.79.012101 PACS number(s): 75.50.Ee, 75.30.Kz, 75.80.+q, 75.40.Mg

Multiferroics are materials that can simultaneously possess electric and magnetic orderings.[1] Such a class of compounds exhibits a magnetoelectric (ME) coupling that is of high technological relevance, since it implies that electrical properties are affected by a magnetic field or conversely that magnetic properties can be varied by an electric field. Multiferroics have been intensively studied from the 1960s to the 1980s[2–5] then "fell in disgrace" among the scientific community (mostly due to weak ME coefficients) until recently experiencing a huge regain in interest (see Refs. 6–13 and references therein).

$BiFeO_3$ (BFO) is one of the most studied multiferroics, undergoes a paraelectric-to-ferroelectric transition around 1083–1103 K,[3,4] and possesses a magnetic ordering below 625–643 K (Refs. 2 and 3) that consists of a cycloidal spin structure superimposed on a *G*-type antiferromagnetism.[14] BFO is thus ferroelectric and exhibits magnetic ordering *at room temperature*, which explains its common denomination as "the holy grail of the multiferroics."[15] However, its intrinsic ME coefficients are very weak,[5,12] which may prohibit its use in various applications. One important problem that remains to be addressed in BFO is the consequence of applying large magnetic fields on the magnetic and electric sublattices, as well as on the ME coupling. As a matter of fact, while the existence of a magnetic transition that destroys the cycloidal structure in favor of a homogeneous magnetic configuration has been proposed in BFO bulks for a critical magnetic field $H_{cyc} \simeq 20$ T (at 20 K),[15,16] we are not aware of any study reporting characteristics of the magnetic ordering and its effects on polarization for fields much higher than H_{cyc}. One may therefore wonder if not only different magnetic transitions can occur at large magnetic field, but also how such transitions (if any) depend on the direction of the applied field and how they affect the polarization.

Motivated to resolve such issues at an *ab initio* level, we developed an effective Hamiltonian from first principles and used it to investigate BFO under magnetic fields applied in the plane perpendicular to the polarization. We report the discovery of striking features, such as a spin-flop transition,[13,17] for which the antiferromagnetic vector suddenly changes in direction while a weak magnetization is created or continuous magnetic transitions that are associated with a large controllable enhancement of the ME coupling.

Our scheme is based on the generalization of the effective Hamiltonian of Ref. 12 to include magnetic *anisotropies* and spin-orbit effects. The total energy E_{tot} is written as a sum of two main terms $E_{\text{FE-AFD}}(\{\mathbf{u}_i\},\{\eta\},\{\omega_i\})$ and $E_{\text{MAG-ANI}}(\{\mathbf{m}_i\},\{\mathbf{u}_i\},\{\eta\},\{\omega_i\})$, where $\mathbf{u}_i$ is the local soft mode in unit cell i (which is directly proportional to the electrical dipole centered on that site) and $\{\eta\}$ is the strain tensor.[18] $\{\omega_i\}$ is a vector characterizing antiferrodistortive (AFD) motions in unit cell i while $\mathbf{m}_i$ is the magnetic dipole centered on the Fe-site i. Practically, $E_{\text{FE-AFD}}$ is the energy provided in Ref. 19 and involves terms solely associated with ferroelectricity (e.g., long-range and short-range effects), strains and AFD motions, as well as mutual couplings between these three latter degrees of freedom. On the other hand, $E_{\text{MAG-ANI}}$ gathers magnetic degrees of freedom and their couplings and is presently proposed to have the following expression:

$$\begin{aligned} E_{\text{MAG-ANI}}(\{\mathbf{m}_i\},\{\mathbf{u}_i\},\{\eta\},\{\boldsymbol{\omega}_i\}) &= \sum_{i,j}\sum_{\alpha,\gamma} Q_{ij,\alpha\gamma} m_{i,\alpha} m_{j,\gamma} + \sum_{i,j}\sum_{\alpha,\gamma} D_{ij,\alpha\gamma} m_{i,\alpha} m_{j,\gamma} \\ &+ \sum_{i,j}\sum_{\alpha,\gamma,\beta,\delta} E_{ij,\alpha,\gamma,\beta,\delta} m_{i,\alpha} m_{j,\gamma} u_{i,\beta} u_{i,\delta} \\ &+ \sum_{i,j}\sum_{\alpha,\gamma,\beta,\delta} F_{ij,\alpha,\gamma,\beta,\delta} m_{i,\alpha} m_{j,\gamma} \omega_{i,\beta} \omega_{i,\delta} \\ &+ \sum_{i,j}\sum_{l,\alpha,\gamma} G_{ij,l,\alpha,\gamma} \eta_l(i) m_{i,\alpha} m_{j,\gamma}, \end{aligned} \tag{1}$$

where the sums over α, γ, β, and δ run over Cartesian components, with the x, y, and z axes being along the [100], [010], and [001] directions, respectively. The sums over i run over all the Fe sites while the sums over j run over the first-, second-, and third-nearest neighbors of the Fe-site i—at the sole exception of the first term where the sum over j runs over *all* the Fe sites. $\eta_l(i)$ is the lth component, in Voigt notation, of the strain at the site i. The first term of Eq. (1) represents the dipolar interactions between magnetic moments,[18] while the second term characterizes magnetic exchanges. The last three terms represent the coupling between magnetism and the local soft modes, AFD degrees of freedom, and strain, respectively. The differences between the present method and the one of Ref. 12 are that not only the long-range magnetic interactions are incorporated here but

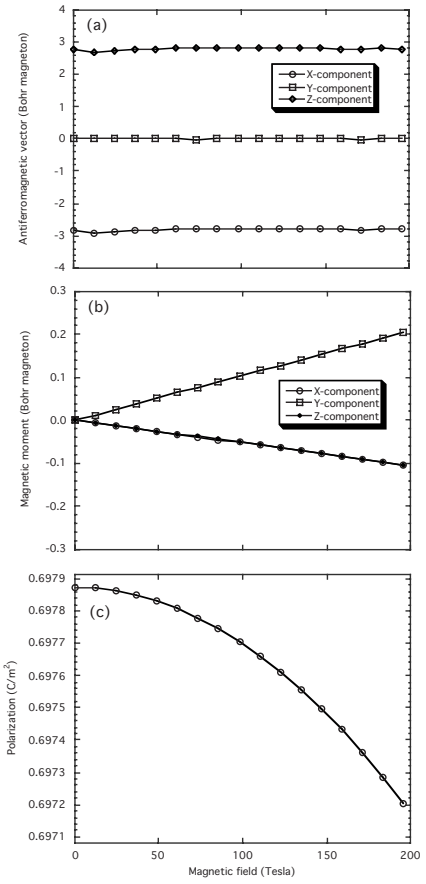

FIG. 1. (a) Antiferromagnetic moment, (b) magnetic moment, and (c) polarization of BFO at 20 K as a function of a magnetic field applied along the $[\bar{1}2\bar{1}]$ direction. The x and z components of **M** are equal to each other for any field.

also that the $D_{ij,\alpha\gamma}$, $E_{ij,\alpha,\gamma,\beta,\delta}$, $F_{ij,\alpha,\gamma,\beta,\delta}$, and $G_{ij,l,\alpha\gamma}$ matrices are dependent on Cartesian axes.[20] Such differences naturally guarantee that magnetic anisotropies are explicitly taken into account, in general, and that Eq. (1) allows the prediction of the angle formed by magnetic and electric dipoles, in particular. The matrices entering the analytical expression of $E_{\text{MAG-ANI}}$ are determined by performing LSDA+U calculations[21,22] (with spin-orbit corrections and noncollinear magnetism) on antiferromagnetic and ferromagnetic supercells, adopting the self-consistent value of 3.8 eV for U—that arises from the application of the proposed scheme of Ref. 23 to BFO. On the other hand, the parameters of $E_{\text{FE-AFD}}$ are those used in Ref. 12 and were extracted from local-density approximation LDA+U computations (with U =3.8 eV). E_{tot} is used in Monte Carlo (MC) simulations on $12\times12\times12$ supercells (8640 atoms) and with up to 4×10^6 MC sweeps to get converged results at any finite temperature. The $\{\mathbf{m}_i\}$'s are assumed to have a fixed magnitude of $4\mu_B$, as consistent with first-principles computations.[10] Relevant outputs of the MC procedure are the polarization **P**, the averaged magnetic-dipole moment **m**, the G-type antiferromagnetic vector **L**, and a vector $\langle\omega\rangle_R$, characterizing AFD motions associated with the R point of the cubic first Brillouin zone.[12,19]

Using this approach yields a Curie temperature of

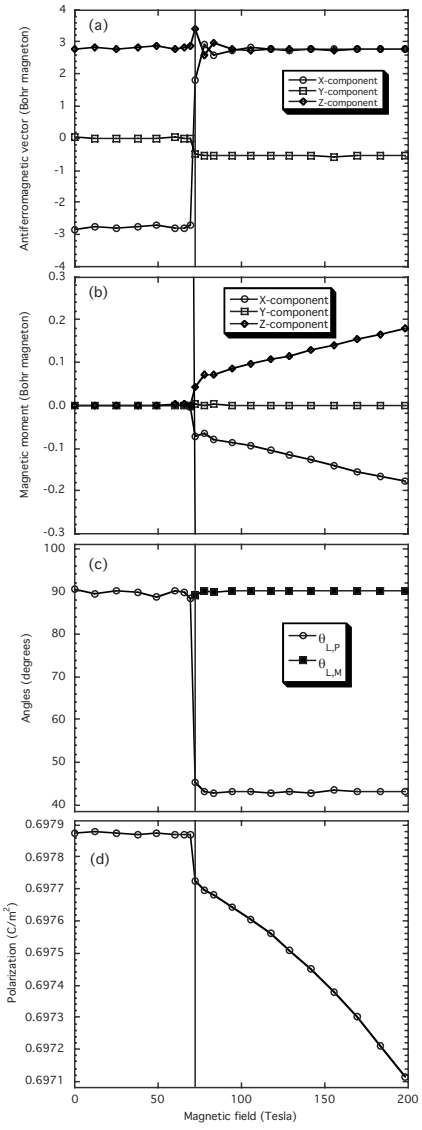

FIG. 2. (a) Antiferromagnetic moment, (b) magnetic moment, (c) angle between antiferromagnetic vector and polarization ($\theta_{L,P}$), (c) angle between antiferromagnetic vector and magnetization ($\theta_{L,M}$), and (d) polarization of BFO at 20 K as a function of a magnetic field applied along the $[\bar{1}01]$ direction.

1080 ± 10 K and a Néel temperature of 660 ± 10 K, which are in excellent agreement with the measurements of 1083–1103 K (Refs. 3 and 4) and $\simeq$625–643 K.[2,3] Our scheme further predicts a *R3c ground state* that exhibits (i) a polarization pointing along the [111] direction; (ii) a tilting of the oxygen octahedra about the [111] axis; and (iii) a G-type antiferromagnetism with **L** lying along the $[\bar{1}01]$ direction, that is, along a $\langle101\rangle$ direction that is *perpendicular* to the polarization. Such predictions are consistent with both first-principles calculations[10,11] and experiments (see Refs. 7 and 11 and references therein). Note that our effective Hamiltonian does *not* yield any weak ferromagnetism at low temperature in BFO bulks. This is in agreement with experiments but contrasts with the *ab initio* study of Ref. 24 that proposed the existence of a weak ferromagnetism due to a spin canting. Note also that BFO *bulk* is in fact *nearly*

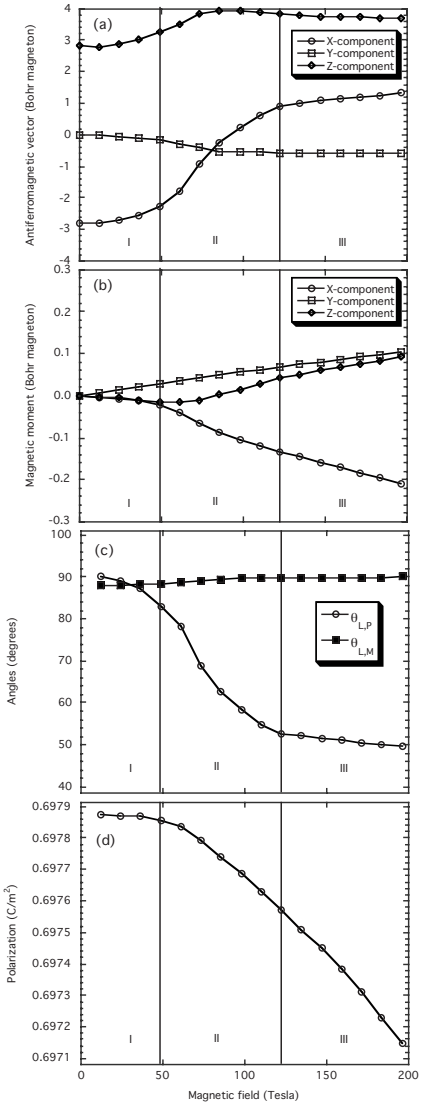

FIG. 3. Same as Fig. 2 but for a magnetic field applied along the $[\bar{2}11]$ direction. I, II, and III denote the three regions discussed in the text.

G-type antiferromagnetic, since a cycloidal spiral arrangement of the magnetic moments with a length of 620 Å has also been reported.[14] Such spiral structure disappears in BFO bulk for a critical magnetic field $H_{\mathrm{cyc}} \simeq 20$ T (at 20 K) and is not found in our simulations [because it either requires the use of much larger supercells or additional interactions in Eq. (1)]. Our results to be discussed below should thus be taken for magnetic fields larger than H_{cyc} in BFO bulk, or for thick films (that do not possess such spiral structure).

Let us now apply, at 20 K, a magnetic field along the $[\bar{1}2\bar{1}]$ direction, that is, along a direction that is perpendicular to both **P** and **L** [the application of a magnetic field is mimicked by adding a dot product between this field and the $\{\mathbf{m}_i\}$'s (Ref. 17) to E_{tot}, and we consider fields of magnitude up to 200 T—which is a large but experimentally accessible value[25]]. Figures 1(a) and 1(b) indicate that such field leaves **L** relatively unchanged, while it induces a weak magnetization along the $[\bar{1}2\bar{1}]$ (field) direction that linearly increases in magnitude as the field increases. The polarization continues to lie along the [111] direction, implying that **M**, **L**, and **P** forms a direct triad, as in the Dzyaloshinksy-Moriya model.[24,26,27] However, its magnitude quadratically decreases as the field increases [see Fig. 1(c)] with a quadratic ME coefficient of $-1.74 \pm 0.01 \times 10^{-8}$ C/T^2 m^2 [the data of Fig. 1(c), as well as any **P**-versus-magnetic-field curve presently studied, can be very well fitted *without* the need to introduce any linear ME coefficient]. Such a weak value is in remarkable agreement with the magnitude of 1.9×10^{-8} C/T^2 m^2 experimentally determined[5] for the quadratic β_{311} coefficient of BFO at 4.2 K (with the "1," "2," and "3" axes being along the $[\bar{1}2\bar{1}]$, $[\bar{1}01]$, and [111] directions, respectively), which further emphasizes the high accuracy of our scheme.

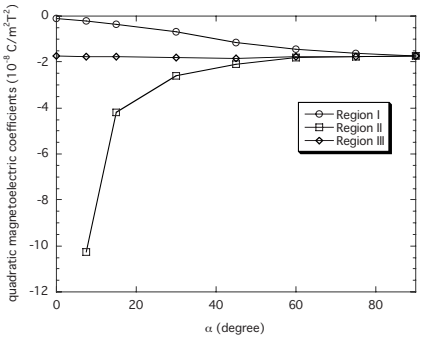

FIG. 4. Quadratic magnetoelectric coefficients of BFO at 20 K, as a function of the angle α formed by the initial direction of the antiferromagnetic vector and a magnetic field applied in the plane perpendicular to the polarization's direction. Regions I, II, and III adopt their own coupling coefficient when $0° < \alpha < 90°$.

Interestingly, Fig. 2 reveals that applying a magnetic field along the ground-state direction of **L** (that is, $[\bar{1}01]$) dramatically affects the magnetic and electric sublattices. More precisely, both **L** and **P** are both nearly unresponsive to the field and no magnetization is created, when the field's magnitude ranges between 0 and $H_{\mathrm{sf}} \simeq 73$ T at 20 K. At this critical value, **M** is *suddenly* induced along the field's direction, while **L** suddenly changes in direction now forming an angle of $\simeq 42°$ with respect to the [111] (polarization) direction in order that **L** is orthogonal to **M**. In other words, the magnetic sublattice of BFO undergoes the so-called spin-flop process.[17,28] (Note that the spin-flop transition reported in Ref. 13 differs from ours in the sense that it is induced by an electric field while our transition originates from the application of a magnetic field.) Such transition has a great impact on the polarization, since this latter exhibits a discontinuity at H_{sf} and then quadratically decreases with the field above H_{sf} with a governing ME coefficient of $-1.75 \pm 0.01 \times 10^{-8}$ C/T^2 m^2 [see Fig. 2(d)].

Due to the difference of the magnetic and electric behaviors between Figs. 1 and 2,[29] one may wonder what happens if the applied magnetic field lies *in between* the $[\bar{1}2\bar{1}]$ and $[\bar{1}01]$ directions. Let us denote by α the angle formed by the direction of this in-plane magnetic field with $[\bar{1}01]$. Figure 3 provides details about magnetic and ferroelectric orders in BFO at 20 K for a particular case (namely, when $\alpha = 30°$, which corresponds to the $[\bar{2}11]$ direction). *Three* different

regions (to be denoted as regions I, II, and III) exist when α is in between 0° and 90°, unlike the *single* region occurring when the field is along $[\bar{1}2\bar{1}]$ [for which **M** lies along the field, see Fig. 1(b)] or unlike the *two* regions associated with a field along $[\bar{1}01]$ [for which **M** is null, and then lies along the field, see Fig. 2(b)]. Region I occurs at low fields and is characterized by **L** still lying close to $[\bar{1}01]$ and by a weak-induced **M** that is nearly perpendicular to **L** (and therefore deviating from the field's direction). In contrast, region III happens at the largest fields and is characterized by **M** now lying along (or close to) the field and also by **L** that is aligned along a direction differing from its ground-state direction (in order that **L** continues to be perpendicular to **M**). Region II is a transitional region, with both **L** and **M** *continuously* rotating with the field's magnitude, under the constraint that they remain perpendicular to each other. What is remarkable is that each region is associated with its own quadratic behavior of the polarization (that is found to always lie along, or extremely near, the [111] direction) versus the magnetic field, as can be seen from Fig. 3(d). For instance, for $\alpha=30°$, region I has a quadratic ME coefficient of $\simeq -0.70\times10^{-8}$ C/T^2 m^2 that is smaller in magnitude than the one of $\simeq -1.8\times10^{-8}$ C/T^2 m^2 associated with region III; while the intermediate region II possesses the highest quadratic ME coefficient—that is, $\simeq -2.6\times10^{-8}$ C/T^2 m^2. Moreover, Fig. 4 displays the ME coefficients of these three different regions as functions of α.[30] The quadratic ME coefficient of region III is nearly independent of α, while the coupling coefficient of region I decreases in magnitude until vanishing [as consistent with Fig. 2(d)] when α decreases from 90° to 0°. The most remarkable feature displayed by Fig. 4 is the dramatic sensitivity of the quadratic ME coefficient associated with region II. Such a latter coefficient quickly increases in magnitude when α is decreased and adopts rather large values for small angles (when $\alpha=7.5°$, this coefficient is around six times larger in magnitude than the one of region III). Our study thus reveals that ME coupling can be controlled and even greatly optimized via a continuous magnetic transition, if one applies a magnetic field lying near (but not along) the initial direction of **L**. We are thus confident that our study leads to a better knowledge of the fascinating multiferroics and hope that it is of technological interest for designing devices based on the cross coupling between magnetic and electric degrees of freedom.

We acknowledge support from ONR under Grants No. N00014-04-1-0413 and No. N00014-08-1-0915, NSF under Grants No. DMR-0701558, No. DMR-0404335, and No. DMR-0080054 (C-SPIN), and DOE under Grant No. DE-FG02-05ER46188. Some computations were made possible thanks to the support provided by the HPCMO of the U.S. DoD and thanks to MRI under Grants No. 0421099 and No. 0722625 from NSF. We thank J. Iniguez for useful discussions.

[1] G. A. Smolenskii *et al.*, Sov. Phys. Usp. **25**, 475 (1982).
[2] P. Fischer *et al.*, J. Phys. C **13**, 1931 (1980).
[3] S. V. Kiselev *et al.*, Sov. Phys. Dokl. **7**, 742 (1963); G. A. Smolenskii *et al.*, Sov. Phys. Solid State **2**, 2651 (1961).
[4] J. R. Teague *et al.*, Solid State Commun. **8**, 1073 (1970).
[5] C. Tabares-Munoz *et al.*, Jpn. J. Appl. Phys., Suppl. **24-2**, 1051 (1985).
[6] J. Wang *et al.*, Science **299**, 1719 (2003).
[7] R. Haumont *et al.*, Phys. Rev. B **73**, 132101 (2006).
[8] R. Palai *et al.*, Phys. Rev. B **77**, 014110 (2008).
[9] N. A. Hill, J. Phys. Chem. B **104**, 6694 (2000).
[10] J. B. Neaton *et al.*, Phys. Rev. B **71**, 014113 (2005).
[11] T. Zhao *et al.*, Nature Mater. **5**, 823 (2006).
[12] I. A. Kornev *et al.*, Phys. Rev. Lett. **99**, 227602 (2007).
[13] D. Lebeugle *et al.*, Phys. Rev. Lett. **100**, 227602 (2008).
[14] I. Sosnowska *et al.*, Physica B **180-181**, 117 (1992).
[15] A. M. Kadomtseva *et al.*, Phase Transitions **79**, 1019 (2006).
[16] Y. F. Popov *et al.*, Low Temp. Phys. **27**, 478 (2001).
[17] L. D. Landau *et al.*, *Electrodynamics of Continuous Media* (Butterworth Heinemann, Oxford, 1984).
[18] W. Zhong *et al.*, Phys. Rev. Lett. **73**, 1861 (1994); Phys. Rev. B **52**, 6301 (1995).
[19] I. A. Kornev *et al.*, Phys. Rev. Lett. **97**, 157601 (2006).
[20] Note that the long-range magnetic interactions are not found to have any significant effect on the phenomena investigated here. These long-range magnetic interactions are nevertheless included for the sake of completeness.
[21] V. I. Anisimov *et al.*, J. Phys.: Condens. Matter **9**, 767 (1997).
[22] G. Kresse *et al.*, Phys. Rev. B **47**, 558(R) (1993); G. Kresse *et al.*, *ibid.* **54**, 11169 (1996).
[23] M. Cococcioni *et al.*, Phys. Rev. B **71**, 035105 (2005).
[24] C. Ederer *et al.*, Phys. Rev. B **71**, 060401(R) (2005).
[25] M. H. Matsuda *et al.*, Rev. Sci. Instrum. **73**, 4288 (2002).
[26] I. Dzyaloshinsky, J. Phys. Chem. Solids **4**, 241 (1958).
[27] T. Moriya, Phys. Rev. **120**, 91 (1960).
[28] The critical field at which the spin-flop process occurs depends on temperature. For instance, H_{sf} reduces from 73 to 60 T when increasing the temperature from 20 to 200 K.
[29] The difference between Figs. 2 and 3, as well as the various effects related to the application of a magnetic field along several *different* directions, to be discussed in Figs. 3 and 4 would not of course have been possible to determine if one uses the effective Hamiltonian approach of Ref. 12 that neglects magnetic anisotropy.
[30] We numerically found that region I always extends from 0 to $\simeq$50 T when $0°<\alpha<90°$ at 20 K. On the other hand, region II first expands when α is increased from 0° to 45° and then shrinks until vanishing (in favor of region III) when further increasing α up to 90°.